Equilibrium and nonequilibrium Lyapunov spectra for dense fluids and solids

Harald A. Posch
Institute for Experimental Physics, University of Vienna, Boltzmanngasse 5, Vienna A-1090, Austria

William G. Hoover
Department of Applied Science, University of California at Davis–Livermore and Lawrence Livermore National Laboratory, Box 808, Livermore, California 94550

(Received 16 August 1988)

The Lyapunov exponents describe the time-averaged rates of expansion and contraction of a Lagrangian hypersphere made up of comoving phase-space points. The principal axes of such a hypersphere grow, or shrink, exponentially fast with time. The corresponding set of phase-space growth and decay rates is called the "Lyapunov spectrum." Lyapunov spectra are determined here for a variety of two- and three-dimensional fluids and solids, both at equilibrium and in nonequilibrium steady states. The nonequilibrium states are all boundary-driven shear flows, in which a single boundary degree of freedom is maintained at a constant temperature, using a Nosé-Hoover thermostat. Even far-from-equilibrium Lyapunov spectra deviate logarithmically from equilibrium ones. Our nonequilibrium spectra, corresponding to planar-Couette-flow Reynolds numbers ranging from 13 to 84, resemble some recent approximate model calculations based on Navier-Stokes hydrodynamics. We calculate the Kaplan-Yorke fractal dimensionality for the nonequilibrium phase-space flows associated with our strange attractors. The far-from-equilibrium dimensionality may exceed the number of additional phase-space dimensions required to describe the time dependence of the shear-flow boundary.

I. INTRODUCTION

Over 100 years ago Boltzmann emphasized the problem of reconciling the irreversible macroscopic behavior of atomistic systems with the time-reversal invariance of the underlying equations of motion.[1] But Boltzmann's H-theorem explanation was criticized because the irreversibility inherent in his equation was based on statistical arguments rather than mechanical principles. Understanding the connection between macroscopic irreversibility and microscopic reversibility has remained a constant challenge. Only recently has a more complete picture been developed.[2–5] The key concepts underlying this understanding are fractal strange attractors and repellors, in phase space, and their relation to the novel nonequilibrium molecular-dynamics simulation techniques made possible by modern supercomputers.[6] Through computer simulation it has finally become possible to extend Boltzmann's H-theorem explanation of irreversibility.

This new understanding of irreversible behavior is based on the phase-space description of nonequilibrium systems. The time development of systems, either at or away from equilibrium, is most concisely described in terms of the phase trajectory in that space. The mathematical stability of the motion, and the quantitative characterization of the irreversibility described by the second law of thermodynamics, require that the motion of a set of contiguous phase points be studied. This set can be visualized as a comoving hypersphere, centered on an ordinary "reference trajectory." The deformation of such a hypersphere then needs to be described. As has been emphasized repeatedly[7] the motion in cases corresponding to a statistical thermodynamic or hydrodynamic description is "Lyapunov unstable." This means that neighboring initial points separate from one another exponentially fast in time. At the same time these "unstable" nonequilibrium motions are actually stable in the sense that they explore only a restricted portion of phase space, a "strange attractor" with a dimensionality less than that of the equilibrium phase space.

Within the limited subspace occupied by the attractor, the trajector comes close to a fractal set of points in the same sense that the Peano curve, shown in Fig. 1, comes close to the points in a two-dimensional unit square. But the mechanism for the covering of the attractor is different from the smaller-and-smaller-scale turnings of a Peano curve. Smale emphasized that phase-space mixing occurs through a "Smale horseshoe" deformation that simultaneously incorporates the expanding and contracting motions characteristic of chaotic time-reversible dynamical systems.[8,9]

These phase-space flows can be partially characterized in terms of their spectrum of Lyapunov characteristic exponents. The results obtained so far for many-particle systems both in equilibrium and nonequilibrium steady states can be summarized as follows.

(1) Equilibrium reversible Hamiltonian systems have Lyapunov spectra made up of pairs $(\pm\lambda)$ that sum to zero. This symmetric distribution, with zero sum, corresponds to the conservation of phase-space volume detailed by Liouville's theorem. As may be verified from

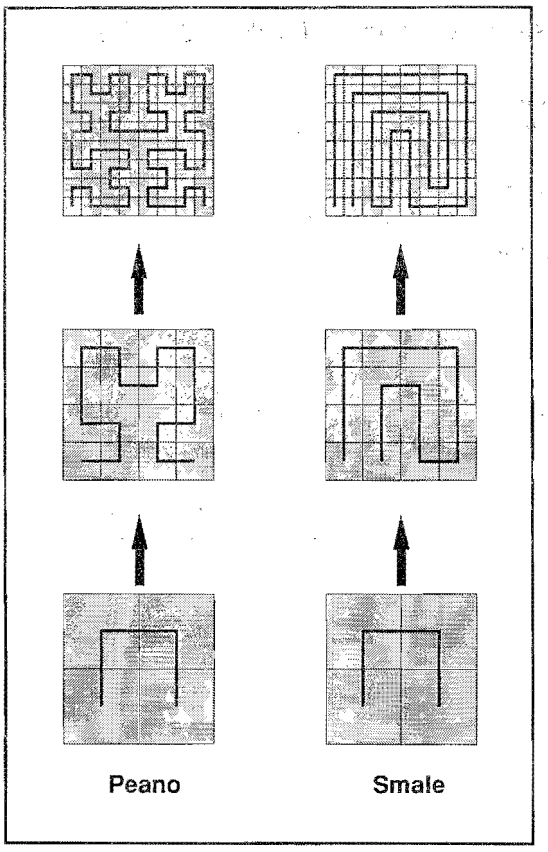

FIG. 1. The Peano space-filling curve and the Smale horseshoe.

Fig. 7 the shape of Lyapunov spectra is typically simple. For either two-dimensional or three-dimensional fluids and solids the equilibrium Lyapunov spectra can be crudely approximated by power laws:

$$\lambda/\lambda_{\max}=(n/n_{\max})^{\beta}\ , \tag{1}$$

where n indexes the $n_{\max}$ pairs of exponents and also represents the number of chaotic degrees of freedom. For three-dimensional fluids β is approximately $\frac{1}{3}$; for solids approximately 1. In two dimensions the corresponding β values are 1 and $\frac{1}{2}$. Because the Lyapunov spectra depend upon the trajectory bifurcations resulting from particle-particle or phonon-phonon collisions, the exponents tend to increase with collision rate. For simple fluids the expected increase with temperature and density has been observed.[5,10]

(2) Away from equilibrium mass, momentum, and energy currents respond to gradients in concentration, velocity, or temperature. Reversible nonequilibrium systems incorporating such flows can be simulated by applying external velocity or temperature perturbations or by imposing an external field. The dissipation associated with such mechanically reversible thermodynamically irreversible flows invariably produces heat, as summarized by the second law of thermodynamics. To achieve a steady state under such nonequilibrium conditions, a thermostatting procedure must be introduced. The thermostat is required to extract the heat energy fed into the system by the external perturbation. Many types of thermostats have been proposed and used in simulations. Theoretically it is desirable that such a thermostat retain the reversible and deterministic character of the fundamental laws of motion. This can be achieved by using either Nosé-Hoover[11–15] or Gaussian[15–19] reversible thermostats. The Nosé-Hoover thermostats have an aesthetic advantage in that, at equilibrium, they generate Gibbs's canonical phase-space distribution. Either type of thermostat is described by time-reversal-invariant equations of motion, a reflection of the Hamiltonian basis they share, as emphasized by Nosé. But neither of these reversible thermostatted sets of motion equations is Hamiltonian.

(3) Lyapunov spectra are insensitive to ensemble, both at and away from equilibrium. At equilibrium completely isolated (microcanonical) systems have spectra very similar to those of thermostatted (canonical or isokinetic) systems. The precise nature of the thermostatting mechanism is immaterial. Our present nonequilibrium results likewise indicate that a similar insensitivity prevails in nonequilibrium systems. Thus, both at and away from equilibrium, the irreversible chaotic motion of N-body systems is insensitive to the choice of statistical ensemble. On the other hand, boundary effects do influence the shape of the spectrum for small systems. Thus periodic systems have simpler Lyapunov spectra than do systems confined by rigid walls.

(4) For steady-state nonequilibrium systems, the symmetry of the Smale pairs of Lyapunov exponents is broken. The sum of each pair of exponents shifts to a negative value, corresponding to a loss of phase-space volume. This means that the phase-space probability density collapses onto a strange attractor, a fractal subspace with zero phase-space volume and with a Kaplan-Yorke fractal dimension significantly smaller than the dimension of the full phase space. In the most extensively studied case, field-driven charge conductivity for a dense fluid,[5] the low-field reduction in phase-space dimension varies as the square of the applied external field. This appearance of a phase-space strange attractor provides a simple and natural explanation for the irreversible behavior of such systems, in accord with the second law of thermodynamics.[2–5] For these reversible nonequilibrium systems Loschmidt's reversibility paradox[20] has thereby been resolved.

The irreversible collapse of the phase-space density onto a strange attractor was first observed in few-body systems described by three-dimensional phase spaces with only three Lyapunov exponents. These investigations included simulations of a periodic two-dimensional isokinetic "Lorentz gas" or "Galton board," driven by an external field,[21] of a one-body one-dimensional Frenkel-Kontorova model for isothermal electronic conduction,[3] and of an isokinetic two-body planar shear flow.[22–24] Further work included the simulation of complete Lyapunov spectra for systems of up to 32 particles in three dimensions, under both equilibrium[25] and nonequilibrium[26,5] conditions. In most of the nonequilibrium work a homogeneous thermostat has been used, with each particle of the system under study subjected to the

thermostatting constraint force. Both Nosé-Hoover thermostats, characterized by a response time τ, and Gaussian thermostats, corresponding to the limit $\tau=0$, have been employed.

Closer to experiment, and therefore of more general interest, are the boundary-bulk-boundary nonequilibrium systems, as indicated schematically in Fig. 2 and investigated earlier.[27,2,4] Such systems may incorporate two or more boundary regions in which particles interact with an external force and a thermostat, with a bulk region sandwiched between the boundaries. In the bulk Newtonian regions the particle motion is solely governed by Newton's equations of motion. In the heat-flow case, with the geometry illustrated in Fig. 3, the boundary regions on the left and right represent hot and cold reservoirs. The heat transported through the Newtonian bulk system can then be studied.[4]

In this paper we present the results of extensive simulations of "two-dimensional" shear flow ("plane Couette flow") for systems of N two- or three-dimensional bulk Newtonian particles. A typical situation is sketched in Fig. 3. The bulk particles are enclosed by a downmoving vertical boundary to the left and an upmoving vertical boundary on the right, with periodic boundaries linking the top and bottom of the system. By fixing the normal separation of the two moving boundaries to a constant value it is possible to describe their horizontal (x) motion with a single degree of freedom, thermostatted by a single Nosé-Hoover thermostat. This model evolved so as to minimize the boundary and thermostat degrees of freedom and is described in more detail in the following section. A modified two-dimensional shear model with two boundary degrees of freedom is discussed in Sec. VI A. Extensions to shear flow in three dimensions are treated in Sec. VI C.

The method for determining the model Lyapunov spectra is discussed in Sec. II. Our simulation results, for systems involving up to $N=81$ bulk particles in two dimensions, and $N=27$ particles in three dimensions, are all reported in Secs. III–VI. As detailed in Secs. IV and VI,

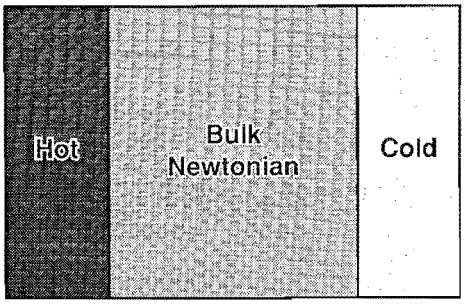

FIG. 2. Schematic illustration of a boundary-driven nonequilibrium steady-state heat-flow simulation. The system is divided into three communicating chambers by vertical walls. Periodic boundaries link the top and bottom boundaries. Particles in the left- (right-) hand region are maintained at a hot (cold) temperature by Nosé-Hoover or Gaussian thermostats. Particles in the Newtonian bulk region transmit heat, on the average, from the hot to the cold region.

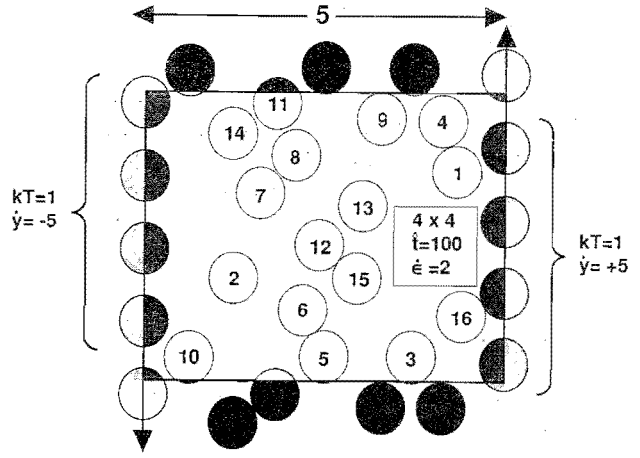

FIG. 3. Snapshot showing a typical 16-particle configuration during a nonequilibrium shear-flow simulation with a strain rate $\dot{\epsilon}=2$. The boundary sites at the left (right) move down (up) ward at a speed $-$ (+) 5. Periodic boundary conditions link the top and bottom of the volume. The thermal temperature of the boundary, in the horizontal direction, corresponds to $kT=1$, as explained in the text. This figure illustrates that the positive shear causes particle collisions to occur preferentially with negative values of $x_{ij}y_{ij}$ making a negative potential contribution to the xy component of the pressure tensor. Here, $\mathbf{r}_{ij}=(x_{ij},y_{ij})$ stands for the vector separating two arbitrary Newtonian particles or a Newtonian particle and a boundary interaction site.

these spectra have shapes qualitatively unlike those found earlier in three dimensions. For two-dimensional fluids, the β of Eq. (1) of $\frac{1}{3}$, found in three dimensions, is instead close to 1. This corresponds to the one-dimensional Debye model, in which the density of k-space states is constant. Further, the presence of nonequilibrium conditions strongly changes the spectrum. The dependence of the Lyapunov spectrum on system size and strain rate is characterized. Section VII contains a discussion of our results and a brief comparison with corresponding model results from continuum hydrodynamics.

II. BOUNDARY-DRIVEN ISOTHERMAL SHEAR FLOW

The geometry of a typical two-dimensional nonequilibrium system is shown in Fig. 3. The bulk Newtonian region consists of N two-dimensional particles of mass m. These interact with each other and with the boundary sites with a short-ranged purely repulsive potential:

$$\phi=\begin{cases}100\epsilon_0[1-(r/\sigma)^2]^4 & \text{if } r<\sigma \\ 0 & \text{if } r\geq\sigma\ .\end{cases} \tag{2}$$

In what follows, including the figures and tables, we use reduced units. The mass m as well as the potential parameters ϵ_0 and σ are unity. We introduced this potential previously[25,26] to eliminate errors from discontinuities in low-order derivatives of ϕ at the cutoff distance $r=\sigma$ (=1).

The Newtonian bulk region is bounded, in the positive and negative x directions, by vertical columns of equally spaced boundary interaction sites (shown as lightly shad-

ed in Fig. 3). These boundary sites are arranged parallel to the vertical (y) axis. The spacing between adjacent boundary sites, σ ($=1$), is equal to the potential cutoff distance. There are L/σ interaction sites for each boundary. L is the periodicity interval for the periodic boundary conditions applied in the vertical direction. The horizontal (x) spacing between centers of the two columns of sites is kept constant and equal to $L+\sigma$. In all simulations L was chosen to be equal to $\sqrt{N}\,\sigma$, thus fixing the number density N/L^2 of the Newtonian bulk particles at 1. All of the boundary sites are coherently joined together, so that their horizontal momentum reacts to the summed interactions of all of the bulk particles which lie within unit distance of any boundary site. The total mass associated with the x motion of the boundary sites is unity, the same as the mass of a single Newtonian bulk particle. The thermodynamic temperature associated with the boundary sites is also taken to be unity, and is enforced by a Nosé-Hoover thermostat which guarantees, on a time-averaged basis, that the fluctuating part of the boundary kinetic energy, $P_x^2/2m$, has the equipartition value, $kT/2=\frac{1}{2}$:

$$\langle P_x^2\rangle/m = kT = 1 \ . \tag{3}$$

Here, P_x is the momentum in the x direction of all $2L$ boundary sites with a combined mass equal to the mass $m=1$ of a Newtonian particle. $\langle\cdots\rangle$ denotes a time average, k is Boltzmann's constant, and T is the average temperature of this horizontal boundary degree of freedom. No thermal fluctuations of the boundary motion in the vertical (y) direction are allowed. In this direction the boundary particles move with a constant velocity V_B related to the imposed strain rate $\dot{\varepsilon}$ by

$$V_B = \dot{Y}_B = \pm\tfrac{1}{2}(L+\sigma)\dot{\varepsilon} \ , \tag{4}$$

where the plus and minus signs refer to the right- and left-hand columns of boundary sites, respectively. It is sufficient to solve the equations of motion for a single boundary site by properly adding all interactions linking bulk and boundary particles using appropriate periodic boundary conditions in the y direction. We denote the position of this reference site by $\mathbf{R}=(X,Y)$, and its fluctuating momentum by $\mathbf{P}=(P_x,0)$. The positions of an arbitrary boundary particle are given by $\mathbf{R}_B=(X_B,Y_B)$. If, furthermore, $\mathbf{r}_n,\mathbf{p}_n$ denote the respective positions and momenta of the bulk particles ($n=1,2,\ldots,N$), then the equations of motion of our model system take the form

$$\begin{aligned}
&\dot{\mathbf{r}}_n = \mathbf{p}_n/m \ , \\
&\dot{\mathbf{p}}_n = -\partial(\Phi_N+\Phi_{\rm int})/\partial\mathbf{r}_n \ , \\
&\dot{X} = P_x/m \ , \\
&\dot{Y} = -(L+\sigma)\dot{\varepsilon}/2 \ , \\
&\dot{P}_x = -\partial\Phi_{\rm int}/\partial X - \zeta P_x \ , \\
&\dot{\zeta} = (P_x^2/mkT-1)/\tau^2 \ .
\end{aligned} \tag{5}$$

Here, Φ_N is the potential energy of the Newtonian bulk (assumed to be pairwise additive), and $\Phi_{\rm int}$ is the interaction energy between the Newtonian particles and the moving walls:

$$\begin{aligned}
\Phi_N &= \sum_{n'\,(<n'')} \sum_{n''} \phi(|\mathbf{r}_{n'}-\mathbf{r}_{n''}|) \ , \\
\Phi_{\rm int} &= \sum_B \sum_{n'} \phi(|\mathbf{r}_{n'}-\mathbf{R}_B|) \ .
\end{aligned} \tag{6}$$

The sum over B is over all $2L/\sigma$ interactions sites of the boundary.

Extension of this model to three dimensions is straightforward. Either spherical or cylindrical boundary particles can be used. We have chosen cylinders to avoid inducing motion in the z direction. This model is discussed in more detail in Sec. VI C.

The thermostat variable ζ, which causes the boundary momentum to fluctuate on a timescale τ in the x direction, is an independent variable arising as a momentum in Nosé's original derivation. Thus, in two (three) dimensions the dimensionality of the phase space is increased from the bulk-particle value of $4N$ ($6N$) to $4N+4$ ($6N+4$) including the x coordinate and momentum of the boundary reference site, its y coordinate, and the friction coefficient ζ. The dimension of the phase space is of crucial importance in the description and discussion of the results of our simulations.

Let the flow equations (5) be abbreviated by

$$\dot{\mathbf{\Gamma}} = \mathbf{G}(\mathbf{\Gamma}) \ , \tag{7}$$

where $\mathbf{\Gamma}=(\mathbf{r}_n,\mathbf{p}_n,X,P_x,Y,\zeta)$ is a $(4N+4)$-dimensional state vector. In principle the $4N+4$ Lyapunov exponents are calculated by solving—in addition to (7)—the $4N+4$ linearized sets of equations[28–32]

$$\frac{d}{dt}(\delta\mathbf{\Gamma})_l \equiv \dot{\delta}_l = \mathbf{D}\cdot\delta_l \ , \tag{8}$$

where $l=1,2,\ldots,4N+4$ for the two-dimensional case. $\mathbf{D}(\mathbf{\Gamma})\equiv\partial\mathbf{G}(\mathbf{\Gamma})/\partial\mathbf{\Gamma}$ is a quadratic dynamical matrix which couples the reference trajectory to the differentially separated satellite trajectories represented by $\delta_l(t)$. An arbitrarily oriented set of orthonormal vectors can serve as initial condition for the vectors $\delta_l(t)$. In the course of time these vectors do not stay orthonormal but tend to rotate into the direction of maximum phase-space growth. By application of a Gram-Schmidt orthonormalization procedure every few time steps one finds that the vector δ_1 tends to point uniquely into a direction of most rapid phase space growth [proportional to $\exp(\lambda_1' t)$]. Similarly δ_1,δ_2 span a subspace whose area grows most rapidly [proportional to $\exp(\lambda_1'+\lambda_2')t$], and so forth. From this sequence all λ_l' are obtained. The Lyapunov exponents are the time averages of these quantities:

$$\lambda_l = \lim_{\hat{t}\to\infty} \frac{1}{\hat{t}} \int_0^{\hat{t}} \lambda_l'(t)\,dt \ . \tag{9}$$

In practice we follow the trajectories forward for a time $\hat{t}$ of the order of 1000 employing a fourth-order Runge-Kutta integration scheme. To avoid initial transients we exclude the first 30% of the trajectory from the averaging procedure. For almost all simulation results we report in the following sections a reduced time step

$\Delta t = 0.001$ is used, all exceptions being specially marked at the appropriate places.

The sum over all Lyapunov exponents ($\sum \lambda$) is equal to the averaged logarithmic rate of growth of the phase-space volume. In our case this means that

$$\langle \Lambda \rangle \equiv \left\langle \frac{\partial}{\partial \Gamma} \cdot \dot{\Gamma}(t) \right\rangle = \sum \lambda = -\langle \zeta \rangle \ , \tag{10}$$

where as in (9) $\langle \cdots \rangle$ denotes a time average (in practice over the length $\hat{\tau}$ of the run). The quantity $\Lambda \equiv (\partial/\partial \Gamma) \cdot \dot{\Gamma}(t)$ is called the phase-space compressibility. The sum rule (10) provides a convenient test for the consistency of our simulation results. Typically (10) is fulfilled to an accuracy of at least four significant digits.

The internal energy of our boundary-bulk-boundary shear problem (5) is given by

$$H(\Gamma) = \Phi_N + \Phi_{\rm int} + \sum_{n'} \frac{\mathbf{p}_{n'}^2}{2m} + \frac{P_x^2}{2m} + \frac{kT}{2} \tau^2 \zeta^2 \ . \tag{11}$$

Making use of the equations of motion the rate of change of $H(\Gamma)$ is given by

$$\dot{H}(\Gamma) = \dot{\Gamma} \cdot \frac{\partial H}{\partial \Gamma} = -kT\zeta + \dot{W}(\Gamma) \ , \tag{12}$$

where

$$\dot{W}(\Gamma) = \sum_B \frac{\partial \Phi_{\rm int}}{\partial Y_B} \dot{Y}_B \ . \tag{13}$$

The sum in the last equation is over all boundary interaction sites, and $\dot{Y}_B$ is given by (4). Since $\partial \Phi_{\rm int}/\partial Y_B$ is the total frictional force component parallel to the shear exerted by the boundary site B on the bulk, $\dot{W}(\Gamma)$ is the rate of work performed on the system by the boundary. The first term on the right-hand side of (12) is the rate at which heat is extracted by the thermostat. In nonequilibrium steady states both terms cancel each other, $\langle \dot{H}(\Gamma) \rangle = 0$, from which we find a quadratic strain-rate dependence of the averaged friction $\langle \zeta \rangle$:

$$\langle \zeta \rangle = \frac{1}{kT} L(L+\sigma) \eta \dot{\varepsilon}^2 \ . \tag{14}$$

In this equation η is the viscosity defined by

$$\left\langle \sum_B \mathrm{sgn}(\dot{Y}_B) \frac{\partial \Phi_{\rm int}}{\partial Y_B} \right\rangle = 2L\eta\dot{\varepsilon} \ . \tag{15}$$

The factor 2 accounts for the total length of the combined left and right boundaries. Equation (14) is used to obtain η from the simulation results for $\langle \zeta \rangle$.

Integrating (12), one finds that the quantity

$$H_{\rm Nosé}(\Gamma) = H(\Gamma) - \int_0^t \dot{W}(\Gamma) dt + kT \int_0^t \zeta \, dt \tag{16}$$

is constant along a trajectory $\Gamma(t)$ both at equilibrium (for which $\dot{W}$ vanishes) as well as in nonequilibrium states. We have verified that $H_{\rm Nosé}$ is indeed conserved by our simulations. However, the total momentum of the boundary-bulk-boundary system is not a constant of the motion.[13] The consequences are discussed in Sec. III.

The information-theory entropy is defined by

$$S_{\rm inf} = -k \int d\Gamma \, f(\Gamma, t) \ln f(\Gamma, t) \ , \tag{17}$$

where $f(\Gamma, t)$ is the phase-space distribution function. Equating time averages with ensemble averages over the nonequilibrium ensemble, one finds for the rate of change of $S_{\rm inf}$ (Refs. 33 and 34)

$$\dot{S}_{\rm inf}/k = \langle \Lambda \rangle = -\langle \zeta \rangle < 0 \ . \tag{18}$$

For nonequilibrium steady-state conditions the rate of change of $S_{\rm inf}$ is balanced by the rate of (global) irreversible entropy production,

$$\dot{S}/k = -\dot{S}_{\rm inf}/k = \langle \zeta \rangle > 0 \ , \tag{19}$$

which according to (14) is a positive quadratic function of the applied strain rate $\dot{\varepsilon}$.

The thermostat response time τ enters the Nosé equations of motion as a free parameter. In what follows we require that τ is proportional to the mean collision time between bulk particles and the boundary. Because in two dimensions the respective collision rate is proportional to the periodicity interval in the y direction, L, we choose $\tau = 1/L$ (in our reduced units). In three dimensions, $\tau = 1/L^2$. The Lyapunov spectra reported in the following sections are insensitive to this choice. Furthermore, the boundary thermostat temperature T chosen for all our simulations corresponds to $kT = 1$.

The linear differential equation for Y in (5) is associated with a vanishing Lyapunov exponent. From a practical point of view it is advantageous to avoid the time-consuming computation of this vanishing exponent in an ordered sequence, $\lambda_i \geq \lambda_{i+1}$, as required by the algorithms. This can be achieved by replacing this trivial differential equation by its integral $Y(t) = Vt + Y(0)$ and using $Y(t)$ for the evaluation of $\Phi_{\rm int}$. This converts the autonomous system of flow equations (5) with $(4N+4)$dimensional phase space into a nonautonomous system of order $4N+3$ and reduces the number of exponents to be calculated by one. In three dimensions $4N$ is replaced by $6N$.

At relatively high strain rates the kinetic energy of some Newtonian particles might become large enough to overcome the potential barrier imposed by the walls. In this case a Newtonian particle can escape by slipping between two neighboring boundary interaction sites. In our first runs we were alerted to this problem by noticing that pairs of Lyapunov exponents started to vanish, two pairs for each escaped particle. We then prevented such escapes by imposing an elastic reflection whenever a bulk particle attempted to cross the boundary lines $x = X$ and $x = X + L + \sigma$, respectively.

III. MAXIMUM LYAPUNOV EXPONENTS

The maximum Lyapunov exponent $\lambda_{\rm max}$ reflects the rate of the fastest dynamical events taking place in phase space. In Table I this quantity is listed for the two-dimensional simulations for various system sizes N both at equilibrium ($\dot{\varepsilon} = 0$) as well as in nonequilibrium steady states. Also given in this table is the time-averaged ther-

TABLE I. Parameters for two-dimensional equilibrium systems ($\dot{\epsilon}=0$) with various system sizes N. The particle density is 1. $\langle K\rangle$ is the kinetic energy of the Newtonian bulk particles and T_N their temperature. $\langle\Phi\rangle$ is the total potential energy (including boundary-bulk interactions). The mean kinetic energy of the boundary is 0.50 in accordance with a boundary temperature given by $kT=1$; $\hat{\tau}$ is the duration of the run with a time step 0.001; λ_{max} is the maximum Lyapunov exponent, and h_K is the Kolmogorov entropy, the sum of the positive Lyapunov exponents; d_L is the "Lyapunov dimension" which—for mixing equilibrium systems—is equal to the number of variables necessary to uniquely define the microscopic system state. The estimated uncertainty for λ_{max} is $\pm 0.6\%$.

					$\dot{\epsilon}=0$				
	$N=4$	$N=9$	$N=16$	$N=25$	$N=36$	$N=49$	$N=64$	$N=81$	$N=100$
$\langle K\rangle$	4.0	9.0	15.4	25.3	35.9	50.6	65.0	81.2	98
$\langle\Phi\rangle$	1.5	4.2	7.3	11.9	16.7	23.3	29.7	37.5	45
kT_N	1.00	1.00	0.96	1.01	1.00	1.03	1.02	1.00	0.98
$\hat{\tau}$	8000	1010	1600	2000	1100	1300	1300	2000	460
λ_{max}	2.73	3.03	3.16	3.29	3.35	3.41	3.47	3.49	3.5
h_K			31		137				
d_L	19	39	67	103	147	199	259	327	403

mostat friction coefficient $\langle\zeta\rangle$ and the peculiar kinetic energy per bulk particle defined by

$$\tilde{K}/N=\sum_n[\mathbf{p}_n-\tilde{\mathbf{p}}(\mathbf{r}_n)]^2/2mN\ . \tag{20}$$

$\tilde{\mathbf{p}}(\mathbf{r}_n)=m\dot{\epsilon}[x_n-X-(L+\sigma)/2]\hat{\mathbf{y}}$ is the momentum at the position of particle n corresponding to a linear velocity profile between the moving boundaries, where $\hat{\mathbf{y}}$ is the unit vector in the y direction. $\tilde{K}/N$ is equal to $k\tilde{T}$, the peculiar temperature of the Newtonian bulk. It should be kept in mind, however, that this definition is based on the assumption of a linear velocity profile, which is not necessarily correct.[35] In general $\tilde{T}$ can differ from the thermostat temperature T for nonequilibrium conditions.

Consulting Fig. 4 one finds that λ_{max} increases logarithmically with system size N both at equilibrium as well as in nonequilibrium steady states. This result also persists if the "free volume" due to the roughness of the boundary is taken into account which reduces the density by 4% for $N=4$ and by 2% for $N=16$. These corrections for the density[5] are too small to affect the logarithmic dependence of λ_{max} with N.

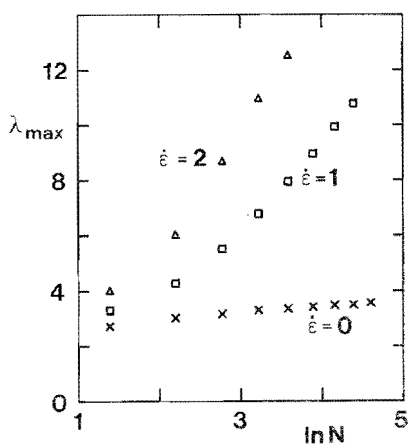

FIG. 4. The maximum Lyapunov exponent λ_{max} as a function of the logarithm of the system size for equilibrium systems ($\dot{\epsilon}=0$, crosses) and nonequilibrium steady states ($\dot{\epsilon}=1$, squares; $\dot{\epsilon}=2$, triangles).

For equilibrium systems ($\dot{\epsilon}=0$) a logarithmic system-size dependence of λ_{max} is not totally unexpected. It is well known that there is a formal analogy between the viscous stress due to velocity gradients in incompressible fluids and elastic stress due to displacement gradients in harmonic solids.[36] The fastest mechanism which determines λ_{max} for a crystal is phonon-phonon scattering.[37] The cross section for this phonon-phonon interaction is proportional to the mean-squared displacement of a typical particle from its lattice site. It has been shown by lattice-dynamical simulations of small two-dimensional crystals composed of N particles[36] that the mean-squared displacement increases as $\ln N$. The proportionality coefficient agrees exactly with that estimated from continuum elastic theory. By invoking this analogy between elastic and viscous stress a logarithmic dependence of λ_{max} on the system size could be expected also for a two-dimensional fluid. This is consistent with our simulations.

It is interesting to note that Stoddard and Ford,[10] in their pioneering numerical study of the mixing behavior of dilute Lennard-Jones gases, estimate a logarithmic dependence of λ_{max} on system size for planar systems. Their arguments are based on a crude kinetic theory of hard disks.

The relation between λ_{max} for a fluid and the mean-square displacement of an appropriate solid should also hold in three dimensions. We have previously shown[5] that λ_{max} for a three-dimensional fluid system does not depend on the system size. This is in agreement with the constant limiting value for the mean-squared displacement of a related solid in three dimensions. In one dimension there appears to be much less number dependence.[38,39]

For nonequilibrium steady-state conditions (with fixed strain rate $\dot{\epsilon}>0$) the relative kinetic energy per particle $\tilde{K}/N$ does not stay constant if the system size is increased. As a consequence, the slope of the graphs of λ_{max} versus $\ln N$ increases with $\dot{\epsilon}$ as depicted in Fig. 4.

An interesting but unexpected phenomenon takes place for larger strainrates ($\dot{\varepsilon}=2$) and large enough systems ($N>36$). It has been mentioned already in Sec. II that the equations of motion (5) do not conserve the total momentum of the boundary-bulk-boundary system:

$$\frac{d}{dt}\left[\sum_n \mathbf{p}_n+\mathbf{P}\right]=\begin{bmatrix}-\zeta P_x\\ -\sum_n \partial\Phi_{\rm int}/\partial y_n\end{bmatrix}. \tag{21}$$

The nonvanishing x component causes a slow drift of the whole system along the x axis without affecting the results. Because of the nonconserved y component of the momentum, it is possible, however, that the Newtonian bulk may lose coupling with a system boundary and start moving with an average velocity equal to that of the left or right boundary. This consequence resembles an order-disorder transition and the maximum Lyapunov exponent quickly drops far below its expected steady-state value. Figure 5(a) shows the time evolution of $\int_0^{\hat{t}}\lambda'(t)dt/\hat{t}$ as a function of the duration of the run, $\hat{t}$, for two simulations of a 49-particle system starting from different initial conditions. One of these trajectories exhibits this sudden transition in the time interval covered by the simulation. An instantaneous snapshot of the fluid structure of such a partially decoupled bulk phase moving along with the right-hand boundary in the positive y direction is shown in Fig. 5(b).

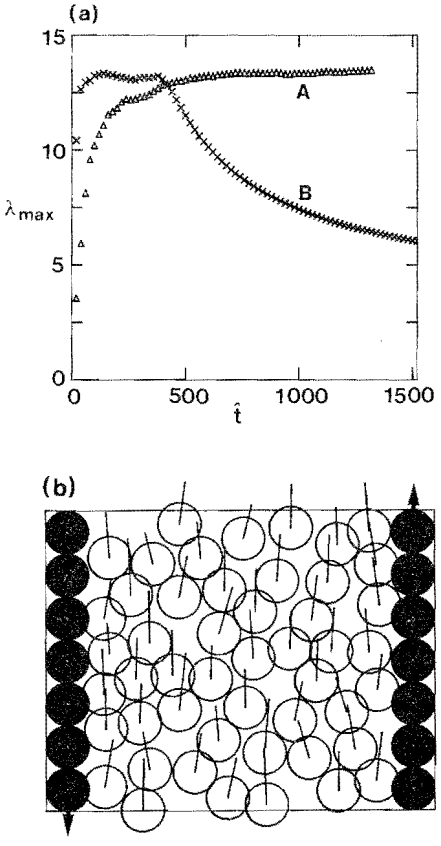

FIG. 5. (a) Curve A shows the convergence of the maximum Lyapunov exponent for a 49-bulk-particle system sheared at a shear rate $\dot{\varepsilon}=2$. $\hat{t}$ is the run time. The same system with different initial conditions suffers a transition into a more ordered state at $\hat{t}$ around 400, which leads to a fast decrease of the maximum Lyapunov exponent as exemplified by curve B. (b) Snapshot of the particle configuration at a run time $\hat{t}=1500$ of curve B in (a). The bars indicate the direction and magnitude of the instantaneous particle velocities. The left (right) boundary moves down (up) with a velocity equal to 8 in reduced units. The particle diameter is $\sigma=1$.

Other kinds of order-disorder transitions have been observed recently in nonequilibrium molecular-dynamics simulations of shear flow both in two[40] and three[41] dimensions. In these simulations momentum-conserving homogeneous thermostats were used. It has been found that for larger shear rates the particles are preferentially arranged along stream lines giving rise to a significant decrease of the viscosity ("shear thinning").

IV. LYAPUNOV SPECTRA FOR TWO-DIMENSIONAL EQUILIBRIUM SYSTEMS

Systems in equilibrium which evolve according to time-reversible equations of motion have symmetric Lyapunov spectra: for each positive exponent there is a corresponding negative one with equal absolute magnitude. The sum over all exponents vanishes indicating conservation of phase-space volume. For such a system it is therefore sufficient to plot only the positive branch of the spectrum, the negative being a mirror image with respect to the abscissa. As an example we show in Fig. 6 the spectrum of a 36-particle system at equilibrium ($\dot{\varepsilon}=0$). Including the boundary and the friction ζ, which vanishes on the average, there are $4N+3=147$ exponents altogether, of which three exponents vanish. All 72 exponents greater than zero are shown in Fig. 6. The abscissa can be thought of as labeling the various ex-

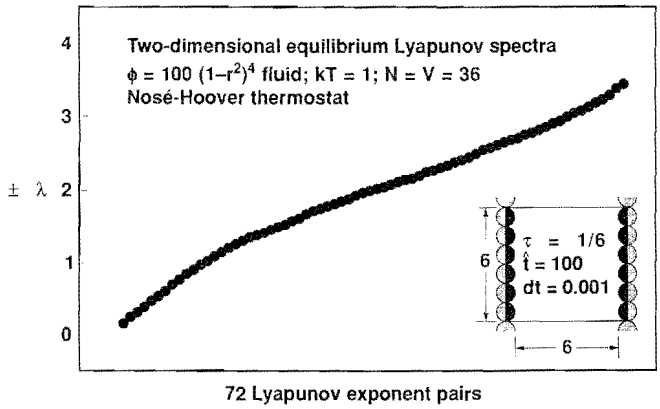

FIG. 6. Lyapunov spectrum for a 36-bulk-particle system in equilibrium ($\dot{\varepsilon}=0$). The boundary Nosé-Hoover thermostat acts in the horizontal x direction and has only one degree of freedom ($g=1$). The thermostat response time is $\tau=\frac{1}{6}$. The time step used for the simulation is equal to 0.001. There are altogether $4N+3=147$ Lyapunov exponents, of which 72 exponents greater than zero are shown in the figure. The negative branch of the spectrum is a mirror image around the abscissa and is not shown. Four vanishing exponents are suppressed. The abscissa indexes the exponents and is not specially labeled.

ponents by a Lyapunov index n, with $n=1$ for the smallest positive exponent and $n=72$ for the top-right maximum exponent λ_{max}. The index $n(\lambda)$ can be interpreted as the number of positive exponents less or equal to λ. Parameters related to this spectrum are also contained in Table I.

This spectrum is relatively simple. But there is no theoretically founded expression describing the shape of the spectrum in Fig. 6. In terms of the empirical formula (1) a linear relation ($\beta=1$) seems roughly appropriate. It is interesting to note that there is a qualitative difference between the shapes of the Lyapunov spectra for fluids and solids both in two (2D) and three (3D) dimensions. The details are shown in Fig. 7:

A. Fluid 2D

This spectrum corresponds to a nine-particle fluid in two dimensions, thermostatted as described in Sec. II and interacting via the potential (2). Relevant parameters are listed in Table I. There are 18 positive exponents in this case.

B. Solid 2D

This spectrum corresponds to an isoenergetic, microcanonical two-dimensional hexagonal solid composed of 12 particles in a cell with periodic boundaries again interacting with the purely repulsive potential (2). The nearest-neighbor separation is 0.9 reduced units corresponding to a reduced particle density of 1.426. The potential and kinetic energies assume the values 10.8 and 5.9, respectively, and the reduced temperature is 0.49. The sum of all positive Lyapunov exponents determines the Kolmogorov entropy and is equal to 8.06 in our reduced units of Sec. II. There are $4N=48$ Lyapunov exponents of which eight vanish. Twenty exponents greater than zero are shown in the figure. The smooth curve is a fit of (1) to these points yielding $\beta=1.6$.

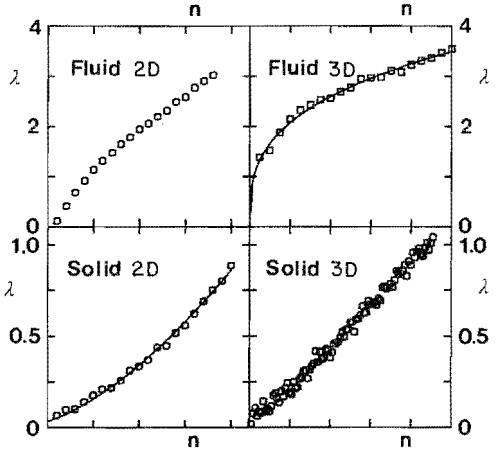

FIG. 7. Comparison of Lyapunov spectral shapes for solids and fluids in equilibrium. The label 2D or 3D indicates whether the system is two or three dimensional. All further information is given in Sec. IV of the main text. As in Fig. 6, only the positive branches of the spectra are shown. The abscisse merely index the exponents and are not labeled.

C. Fluid 3D

This is a Lyapunov spectrum for an eight-particle three-dimensional fluid in isoenergetic equilibrium.[5] The particles interact via a repulsive Lennard-Jones potential and the Lyapunov exponents are given in Lennard-Jones reduced units. Relevant parameters are listed in Table I of Ref. 5 (state I). The smooth curve is a fit of (1) to 20 points greater than zero giving $\beta=\frac{1}{3}$.[5]

D. Solid 3D

This spectrum is for a 32-particle fcc solid in three dimensions and isoenergetic equilibrium.[42] Periodic boundary conditions are employed. The particles interact via a Lennard-Jones (LJ) potential with LJ parameters ϵ_{LJ} and σ_{LJ}. The potential is smoothly truncated at $\sqrt{3}\sigma_{LJ}$ by fitting a cubic spline at the inflection point $(\frac{26}{7})^{1/6}\sigma_{LJ}$. This potential has been used also by Holian and coworkers in their study of fluid viscosity[43] and fragmentation[44] by molecular dynamics. All quantities related to this spectrum are given in LJ-reduced units. The number density is 1.0, and the time-averaged potential and kinetic energies are -175.0 and 26.3, respectively. This corresponds to a reduced temperature $kT=0.55$. The Kolmogorov entropy becomes 46.8. There are $6N-10$ nonvanishing exponents, and 91 exponents greater than zero are plotted in the figure. The data are represented quite well by a straight line corresponding to $\beta=1$ in terms of Eq. (1).

Inspection of the data displayed in Fig. 7 reveals significant qualitative differences in the shape of the spectra for fluids and solids both in two and three dimensions. A fundamental understanding of these results is still missing. It is hoped that at least for solids an interpretation of the spectra in terms of lattice-dynamical concepts will be obtained soon.

V. LYAPUNOV SPECTRA FOR TWO-DIMENSIONAL SYSTEMS IN NONEQUILIBRIUM STEADY STATES

By steadily shearing the planar systems introduced in Sec. II, the symmetry of the Lyapunov spectra is lost. The rate of global entropy production, equal to the time-averaged thermostat variable $\langle\zeta\rangle$ and according to (9) the negative sum of all Lyapunov exponents, must be positive for nonvanishing $\dot{\epsilon}$. In Fig. 8 we show Lyapunov spectra for different system sizes for a shear rate $\dot{\epsilon}=1$. Analogous spectra for $\dot{\epsilon}=2$ are depicted in Fig. 9. The abscissa is given by the Lyapunov index n and has not been labeled in these figures to permit a clear presentation. Only non-negative exponents are plotted. Further relevant information for these runs is collected in Tables II and III. This includes the viscosity, calculated from (14), the Reynolds number

$$\mathcal{N}_{\mathrm{Re}}=\frac{mN}{L^2}\frac{L^2(L+\sigma)^2\dot{\epsilon}^3}{kT\langle\zeta\rangle}\,, \tag{22}$$

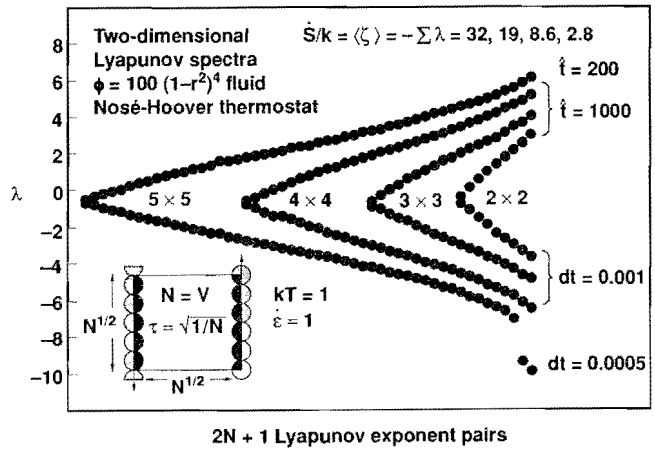

FIG. 8. Two-dimensional Lyapunov spectra for a shear rate $\dot{\epsilon}=1$ and various system sizes as indicated by the label ($N=L\times L$ in reduced units). The boundary thermostat has a single degree of freedom (in the x direction) as outlined in Sec. II. The relevant parameters for these spectra are collected in Table II. Vanishing exponents are not shown. dt is the time step for the simulation and $\hat{t}$ is the length of the run. All parameters are explained further in the text and are given in reduced units. The abscissa merely indexes the exponents and is not labeled.

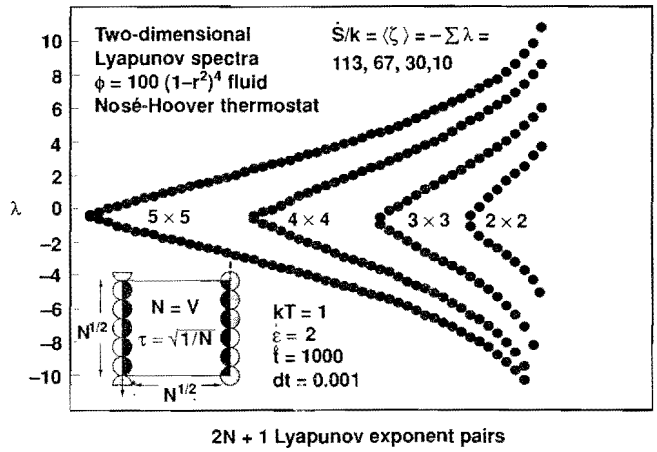

FIG. 9. Two-dimensional Lyapunov spectra for a shear rate $\dot{\epsilon}=2$ and various system sizes as indicated by the label ($N=L\times L$ in reduced units). The boundary thermostat has a single degree of freedom (in the x direction) as explained in Sec. II. Relevant parameters for these spectra are given in Table III. Vanishing exponents are not plotted. For the larger systems some of the most negative exponents are far off the scale of this figure and are not shown but listed in Table III. As usual, the abscissa merely indexes the exponents and is not specially labeled.

and the fractal dimension d_L of phase space discussed below.

When $\dot{\epsilon}$ increases the shape of the spectrum changes in a very pronounced way: the slopes of both the positive and negative branches increase in absolute value. In addition the spectrum is shifted downward. The most positive exponents are increased noticeably. But the most dramatic change takes place with the most negative exponents which become so negative that they do not fit on the scale of Fig. 9. The four most negative exponents are listed in Tables II and III along with $\lambda_{\max}$ for some of the spectra studied.

The asymmetry of the Lyapunov spectra in the nonequilibrium case implies that the sum of all Lyapunov ex-

TABLE II. Parameters for the two-dimensional system sheared at a rate $\dot{\epsilon}=1$. N is the system size, $\tilde{K}$ is the relative kinetic energy of the bulk particles defined in (20). $\langle\zeta\rangle$ is the time-averaged Nosé friction coefficient, η the viscosity defined in (14), and $\mathcal{N}_{\mathrm{Re}}$ is the Reynolds number estimated from (22). The mean kinetic energy of the boundary is 0.50, in agreement with the boundary temperature given by $kT=1$. The density of the bulk $mN/L^2=1$; Δd_L is the loss in phase-space dimensionality as explained in Sec. V. The other parameters are defined in Table I. All quantities are given in reduced units. The four most negative Lyapunov exponents, the Kolmogorov entropy h_K, and Δd_L are taken from a different (shorter) run illustrated in Fig. 8.

	$\dot{\epsilon}=1$							
	$N=4$	$N=9$	$N=16$	$N=25$	$N=36$	$N=49$	$N=64$	$N=81$
$\langle\tilde{K}\rangle/N$	1.8	2.5	4.1	6.3			14.8	17.5
$\langle\Phi\rangle$	3.0	10.6	31.0	74	148	261	436	642
$\hat{t}$	8000	2020	2760	1340	1100	104	1260	1480
$\lambda_{\max}$	3.29	4.28	5.52	6.78	7.95	8.95	9.93	10.8
The four most	−2.3	−3.6	−5.3	−6.4				
negative	−2.6	−4.1	−5.6	−6.7				
Lyapunov	−3.0	−4.4	−5.9	−8.7				
exponents	−3.4	−4.6	−6.3	−9				
h_K	15	40	84	147				
$\langle\xi\rangle$	2.84	8.63	18.7	31.6	46.4	62.0	85.3	114
$\mathcal{N}_{\mathrm{Re}}$	13	17	22	29	38	51	61	71
η	0.48	0.72	0.94	1.05	1.10	1.11	1.18	1.26
Δd_L	0.8	1.9	3.2	4				

TABLE III. Parameters for two-dimensional systems sheared at a rate $\dot{\varepsilon}=2$. All the quantities are defined in Tables I and II and are given in reduced units. The four most negative Lyapunov exponents, the Kolmogorov entropy h_K, and the phase-space reduction Δd_L are taken from a different (shorter) run illustrated in Fig. 9.

	$\dot{\varepsilon}=2$				
	$N=4$	$N=9$	$N=16$	$N=25$	$N=36$
$\langle \tilde{K} \rangle / N$	3.95	7.44	14.3	22.5	40.8
$\langle \Phi \rangle$	5.6	27.2	105	255	431
$\hat{t}$	2020	4050	3020	2040	1550
$\lambda_{\max}$	4.03	6.05	8.70	10.90	12.5
The four most	−3.2	−6.3	−8.6	−9.4	
negative	−3.7	−7.0	−9.5	−10	
Lyapunov	−4.2	−8.1	−12	−11	
exponents	−5.0	−12	−43	−100	
h_K	16	50	117	206	
$\langle \zeta \rangle$	10.0	30.1	67	113	171
$\mathcal{N}_{\mathrm{Re}}$	29	38	48	64	83
η	0.42	0.63	0.84	0.94	1.02
Δd_L	2.2	3.5	3.3	2.2	

ponents, which according to (10) is equal to the averaged phase-space compressibility $\langle \Lambda \rangle$, is always negative. This means that an arbitrary hypervolume in phase space shrinks in the course of time and develops into a very complicated fractal-like subspace. The dimension of this fractal object, d_L, can be obtained from the number of exponents needed for the cumulative sum $\mu(J)=\sum_{i=1}^{J}\lambda_i$ (with $\lambda_i \geq \lambda_{i+1}$) to change sign. According to the Kaplan and Yorke[45] linear interpolation formula one has

$$d_L = J + \frac{\mu(J)}{|\lambda_{J+1}|} , \tag{23}$$

where the integer J is obtained from the conditions $\mu(J)\geq 0$ and $\mu(J+1)<0$.

In Tables II and III we also list the reduction in dimensionality, Δd_L, of the accessible phase-space volume from its equilibrium value caused by the dissipative perturbation $\dot{\varepsilon}\neq 0$. This number is obtained from $\Delta d_L = d_L(0)+1-d_L(\dot{\varepsilon})$, where $d_L(0)$ is taken from Table I, and the addition of 1 accounts for the Y coordinate of the boundary (which in equilibrium is a constant for this model). One immediately notices that Δd_L never exceeds $d_B=4$, the dimension contributed by the boundary degrees of freedom: X, P_x, Y, ζ. This is an interesting and significant result. It means that an increase of the shear rate will result—according to (14) and (15)—in an increase of $\langle \zeta \rangle$ and consequently of η, but the shape of the Lyapunov spectrum changes sufficiently to keep the loss in dimensionality below d_B. This is possible only by still further reducing mainly the last few most negative exponents to produce the necessary reduction in the sum of all exponents. This is precisely what is generally observed. It should be noted in this context that the considerations in Ref. 4 do not apply to the boundary-bulk-boundary problems treated here because of this strange behavior of the most negative exponents. We expect that this shape change would be much less severe if more boundary degrees of freedom were present.

To test whether this result is of a general nature we simulated further shear models, both in two and three dimensions, which differed in the dimension d_B needed to describe the action of the boundary. These results follow in Sec. VI.

VI. MODIFIED SHEAR MODELS IN TWO AND THREE DIMENSIONS

A. Planar Couette flow with a modified Nosé thermostat

We increase the dimension d_B contributed by the boundary thermostat by allowing the boundary interaction sites to fluctuate thermally not only in the x direction (as in Sec. II) but also in the y direction, the direction of the shear. There are two thermostatting degrees of freedom, $g=2$, as compared to one for the model of Sec. II. The equations of motion now assume the form

$$\begin{aligned}
&\dot{\mathbf{r}}_n = \mathbf{p}_n/m \ , \\
&\dot{\mathbf{p}}_n = -\partial(\Phi_N+\Phi_{\mathrm{int}})/\partial \mathbf{r}_n \ , \\
&\dot{\mathbf{R}} = \mathbf{P}/m - \tfrac{1}{2}(L+\sigma)\dot{\varepsilon}\hat{\mathbf{y}} \ , \\
&\dot{\mathbf{P}} = -\partial\Phi_{\mathrm{int}}/\partial \mathbf{R} - \zeta \mathbf{P} \ , \\
&\dot{\zeta} = (\mathbf{P}^2/2mkT - 1)/\tau^2 \ .
\end{aligned} \tag{24}$$

As before, $\mathbf{R}=(X,Y)$ denotes the position and $\mathbf{P}=(P_x,P_y)$ the thermally fluctuating part of the momentum for the boundary reference site. $\hat{\mathbf{y}}$ is the unit vector in y direction. The thermostat temperature is now determined by

$$kT = (P_x^2+P_y^2)/2m \tag{25}$$

instead of (3), and the sum rule (10) takes the form

$$\sum\lambda=-g\langle\zeta\rangle\ , \tag{26}$$

where $\sum\lambda$ is the sum over all Lyapunov exponents. In practice this equation for a 16-particle system is obeyed with a precision of at least five significant figures after 300 000 time steps.

Similar to (16) the quantity

$$H_{\text{Nosé}}(\Gamma)=\Phi_N+\Phi_{\text{int}}+\sum_n\frac{\mathbf{p}_n^2}{2m}+\frac{\mathbf{P}^2}{2m}+\frac{kT}{2}g\tau^2\zeta^2 -\int_0^t\dot{W}(\Gamma)dt+gkT\int_0^t\zeta\,dt \tag{27}$$

($g=2$) is a constant along the trajectory $\Gamma(t)$, where $\dot{W}$ given by (13) is the rate at which work is performed on the system by the boundary. The value of $H_{\text{Nosé}}$ depends on the choice of the time origin. We have verified that (27) is conserved by our simulations. As in the shear model of Sec. II the total momentum is not a constant of the motion.

$4N+5$ variables are needed to characterize uniquely the state vector $\Gamma=(\mathbf{r}_n,\mathbf{p}_n,\mathbf{R},\mathbf{P},\zeta)$ of the system. Consequently the equilibrium phase-space dimension $d_L(0)=4N+5$. The reduction in phase-space dimensionality due to the dissipative perturbation is given by $\Delta d_L=4N+5-d_L(\dot{\epsilon})$. The dimension contributed by the boundary degrees of freedom is $d_B=5$.

Figure 10 shows results of such simulations for systems consisting of $N=4$ and $N=16$ Newtonian bulk particles and a boundary shear rate $\dot{\epsilon}=2$. Relevant parameters are given in Table IV. The shapes of the sheared-fluid spectra are very similar to that for corresponding curves in

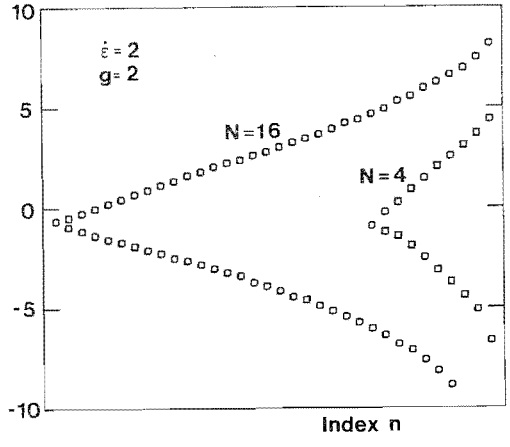

FIG. 10. Full Lyapunov spectra for the modified two-dimensional shear system introduced in Sec. VI under nonequilibrium steady-state conditions $\dot{\epsilon}=2$. In contrast to Figs. 8 and 9, the boundary Nosé-Hoover thermostat has two degrees of freedom ($g=2$). The systems studied have four and 16 bulk particles, respectively. Further relevant parameters are given in Table IV. There are altogether 21 and 69 Lyapunov exponents in these cases, respectively, of which two vanishing exponents are not shown in the figure although they have to be counted in the evaluation of the dimensionality. Some of the most negative exponents do not fit on the scale and are listed in Table IV instead.

TABLE IV. Results for the modified shear model of Sec. VI A. The boundary thermostat has two fluctuating degrees of freedom ($g=2$). All quantities are defined in Tables I and II and are given in reduced units; and $\sum\lambda$ is the sum over all Lyapunov exponents.

	$\dot{\epsilon}=2$	
	$N=4$	$N=16$
$\langle\tilde{K}\rangle/N$	4.1	12.7
$\langle\Phi\rangle$	6.3	79.6
$\hat{\tau}$	2000	1500
$\lambda_{\max}$	4.38	7.85
The five	−3.12	−8.03
most	−3.72	−8.74
negative	−4.40	−11.04
Lyapunov	−5.09	−14.17
exponents	−6.65	−33.46
h_K	18.2	106
$\sum\lambda$	−13.03	−76.11
$\langle\zeta\rangle$	6.52	38.06
$\mathcal{N}_{\text{Re}}$	42	84
η	0.27	0.48
Δd_L	2.61	5.09±0.015

Fig. 9. Of particular interest is the reduction in phase-space dimensionality obtained for $N=16$. The equilibrium phase-space dimension $d_L(0)=69$. Application of a shear with a shear rate $\dot{\epsilon}=2$ reduces this number by $\Delta d_L=5.09\pm0.015$. The phase space contracts towards a fractal subspace with a dimension $d_L=63.91$, a number slightly, but significantly, *smaller* than the dimension $4N=64$ contributed by the Newtonian bulk particles. The standard deviation for Δd_L was estimated by dividing the trajectory into batches of 100 time units each. This example shows that—by perturbing a system with an external boundary—it seems to be possible to obtain a reduction in dimensionality larger than the dimension d_B contributed by the boundary variables and to "cut" into the dimension of the bulk.

Up to now this is the only model system for which we were able to find this important property. Increasing the shear ratio to $\dot{\epsilon}=3$ for this system leads to an order-disorder transition similar to that mentioned in Sec. III and to a significant reduction of Δd_L.

B. Two-dimensional shear models with rectangular basis cells

We have investigated also shear models with basically the same geometry as that shown in Fig. 3 except that the basis cell was not a square but a rectangle with the longer side arranged in the direction of the shear. The systems studied included (i) $N=5$ Newtonian particles arranged in a cell $2\sigma\times5\sigma$, and (ii) $N=10$ Newtonian particles in a cell with dimensions $3\sigma\times5\sigma$. In both cases there are five interaction sites on the up- and down-moving boundaries per periodicity length 5σ. Shear rates up to $\dot{\epsilon}=10$ were examined. In no case was a reduction in dimensionality

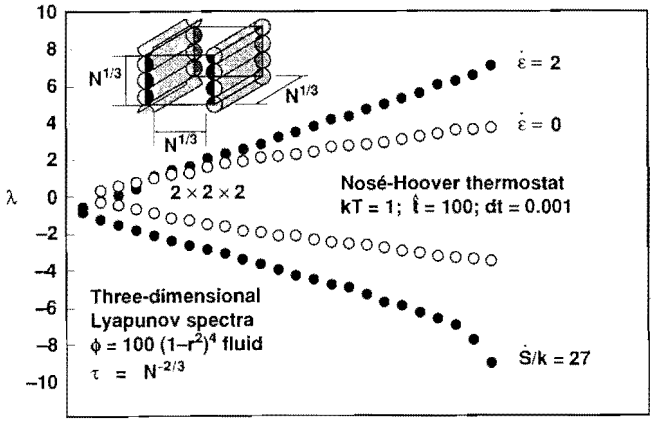

FIG. 11. Lyapunov spectra for the three-dimensional shear model introduced in Sec. VI.

found which exceeded the dimensions d_B contributed by the boundary degrees of freedom.

C. A simple shear model in three dimensions

The model introduced in Sec. II for planar Couette flow can be generalized to three dimensions. Instead of disks, we choose a boundary consisting of cylinders of length L and diameter σ, arranged parallel to the z axis. The cylinders are coherently joined together, fluctuate only in x direction, and move with constant velocity along the positive or negative y directions. The bulk particles interact in x and y directions with interaction sites located on the axes of the cylinders. The geometry is sketched in Figs. 11 and 12. The z component of the momentum becomes a conserved quantity and contributes one vanishing pair of Lyapunov exponents. Just as in two dimensions the nonequilibrium system has one more vanishing exponent pair than the respective equilibrium system.

Lyapunov spectra obtained with this model are depicted in Fig. 11 for $N=8$ and in Fig. 12 for $N=27$. In all cases of three-dimensional shear flows reported here the

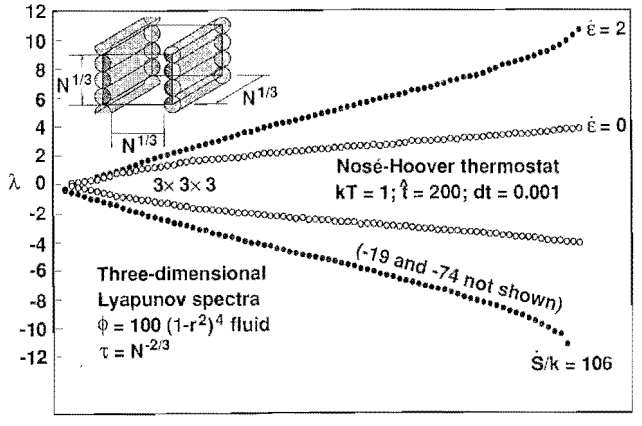

FIG. 12. Lyapunov spectra for the three-dimensional shear model introduced in Sec. VI.

reduction in dimensionality, Δd_L, is again smaller than the dimension d_B contributed by the respective boundary.

VII. DISCUSSION

The equations of motion for all of the systems studied in this paper have an important common feature: they are invariant with respect to time reversal. In spite of this symmetry we observe only trajectories characterized by a positive friction $\langle \zeta \rangle$. In accordance with the second law of thermodynamics, work—performed by the external walls—is always converted into heat, never the reverse. The key for understanding this "arrow of time" based on time-reversal-invariant equations of motion lies[2-5] (a) in the recognition that in nonequilibrium states an arbitrary phase-space volume collapses onto an attracting subspace with fractal dimension d_L smaller than the equilibrium dimension of the phase space (its volume is not just "small"; it vanishes identically); and (b) in the fact that trajectories violating the second law are characterized by $\langle \zeta \rangle < 0$ and must therefore be located *precisely* on the associated repellor. Repellor states could in theory be constructed from the strange-attracting subspace by applying a time-reversal transformation ($\mathbf{q} \to \mathbf{q}$, $\mathbf{p} \to -\mathbf{p}$, $\zeta \to -\zeta$) to it. They would form again a fractal subspace with fractal dimension d_L and vanishing phase-space volume. But because time reversal also changes the sign of all Lyapunov exponents, the repellor states would be characterized by a positive sum of Lyapunov exponents and would therefore be inherently unstable. The slightest deviation would blow up exponentially in time with the trajectory soon ending up on the attractor again. Thus, because of (a) an *exact* localization of the repellor is impossible, and because of (b) the repellor's instability prevents any *approximate* effort to localize and follow a time-reversed trajectory on the repellor.

The geometrical concept of a fractal attractor and repellor in the phase space of nonequilibrium steady-state systems resolves the famous reversibility paradox first formulated by Loschmidt[20] in 1876 and discussed in more detail by Boltzmann.[1] To explain the second law Boltzmann was forced to introduce statistical arguments. Our results indicate that the second law can be understood in purely geometrical terms. It follows from the equations of motion that the rate of work $\dot{W}(\Gamma)$ performed on the system by the boundary is proportional to the logarithmic rate of growth of phase-space volume [Eqs. (10) and (12)]. This phase-space volume may either stay constant, signaling equilibrium, or it may shrink, as is inevitable for systems in nonequilibrium steady states. The possibility of steady phase-space growth corresponding to a positive sum of Lyapunov exponents would imply divergence of the kinetic energy incompatible with a steady state.

Essential to these results is the use of a deterministic time-reversible thermostat. Nosé-Hoover mechanics (including Gauss's isokinetic equations as a special case) is ideally suited for that purpose. In almost all systems studied so far, homogeneous thermostats have been used[5,22-26] where each particle is directly subjected to the

thermostatting constraint force. In this paper, however, we study composite boundary-bulk-boundary nonequilibrium systems, in which only the boundary particles are thermostatted and are exposed to an external perturbing force. The bulk region is composed of particles obeying solely Newton's equations. In addition to all the irreversible properties summarized above we find an important new feature: The reduction of phase-space dimension associated with the irreversible flux can only with great difficulty exceed the dimension d_B necessary to describe the state of the boundary. This important result has been found previously in a study of heat flow from a hot to a cold reservoir,[4] but our shear-flow results presented in this paper make this conclusion much more convincing. For small systems it seems to be difficult to reduce the dimensionality of the attracting subspace for the total system below a limit set by the dimension of the Newtonian bulk particles. Only in one of the systems studied here does the reduction in dimensionality exceed d_B. In contrast to heat conduction[4] the thermostatted boundary strongly influences the attainable phase-space dimensionality loss Δd_L for the shear flow problems studied here.

A new and important role has to be attributed to the few most negative Lyapunov exponents. We have demonstrated in Secs. V and VI that they have a decisive influence both on the sum of all Lyapunov exponents and the dimensionality loss. The most strongly converging directions in phase space therefore largely determine the irreversible behavior. This is in accord with the information-theoretical arguments by Shaw.[46] We have recently shown[47] how the most negative Lyapunov exponents can be calculated without the need to compute the whole spectrum of exponents as required by the classical algorithms. This method also provides the possibility of obtaining negative exponents directly from experimental time series.

Shear flow in two and three dimensions can also be studied by continuum hydrodynamics.[48] Taking the Navier-Stokes equations as a starting point the Lyapunov spectra for planar shear flow at low[49] and high[50,51] Reynolds numbers have been approximated by simulation. Since the dimension of the state space of a partial differential equation is infinite, the problem is numerically approached by introducing a grid of points in phase space (100×100 are typical) and using finite-difference methods or Fourier techniques. The dimensionality of the resulting caricature problem is then determined by the number of variables used in the simulation.

Grappin and Leorat[49] studied low-Reynolds-number flow in two dimensions similar to ours. They reported a complete Lyapunov spectrum in the limit of vanishing viscosity. The shape of this spectrum should be comparable to our equilibrium results in Sec. IV. Because in Ref. 49 only the cumulative sum $\mu(n)=\sum_{i=1}^{n}\lambda_i$ is shown, where as usual $\lambda_i \geq \lambda_{i+1}$, we replot their results in Fig. 13

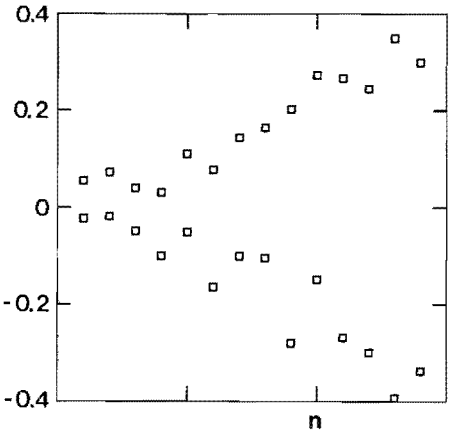

FIG. 13. Lyapunov spectrum of a two-dimensional, zero-viscosity hydrodynamic flow model obtained by Grappin and Leorat (Ref. 49). These authors give the cumulative sum $\mu(n)$ of Lyapunov exponents. To facilitate comparison of the spectral shape with our results in Fig. 7 (Fluid 2D), we have replotted their data in this figure using the reduced units of Ref. 49.

to facilitate this comparison. The shape of the spectrum in Fig. 13 is indeed similar to our results (see, for instance, the panel labeled "Fluid 2D" in Fig. 7) and is described by $\beta=1$ in terms of (1). For nonvanishing η their Lyapunov dimension is of the order of 9 and depends strongly on the wave number of the applied shear.

A much larger dimension has been reported by Yamada and Ohkitani[50] for a turbulent flow, and the shape of their spectra differs qualitatively from our results. For turbulent flow at Reynolds numbers around 2800 only a lower limit can be given for the Lyapunov dimension of the strange attractor ($d_L > 400$).[51]

ACKNOWLEDGMENTS

Work performed at the University of Vienna was supported by the Fonds zur Förderung der wissenschaftlichen Forschung, Contract No. P5455, and by the Computer Centers of the University and the Technical University. Work performed at Lawrence Livermore National Laboratory was carried out under the auspices of University of California–United States Department of Energy Contract No. W-7405-Eng-48. We are specially grateful to Roger Minich, Hans-Peter Axmann, Peter Karlsreiter, and Carol Hoover for their active support. We thank Bill Ashurst, Mike Feit, Dieter Flamm, Dick Grover, Brad Holian, Ray Kapral, Bill Moran, Heide Narnhofer, Walter Thirring, Jim Viecelli, and Tom Wainwright for a variety of stimulating and helpful conversations. We thank Gary Morriss for sending us Ref. 24 prior to publication and for stimulating suggestions.

L. Boltzmann, Sitzungsber. kais. Akad. Wiss. Wien, Math. Naturwiss. Kl. Abt. 2 **75**, 67 (1877).

[2]B. L. Holian, W. G. Hoover, and H. A. Posch, Phys. Rev. Lett. **59**, 10 (1987).

[3]W. G. Hoover, H. A. Posch, B. L. Holian, M. J. Gillan, M. Mareschal, and C. Massobrio, Mol. Simulation **1**, 79 (1987).

[4]W. G. Hoover, Phys. Rev. A **37**, 252 (1987).

[5]H. A. Posch and W. G. Hoover, Phys. Rev. A **38**, 473 (1988).

[6]W. G. Hoover, *Molecular Dynamics,* Vol. 258 of *Lecture Notes in Physics,* edited by H. Araki, J. Ehlers, K. Hepp, R. Kippenhahn, H. A. Weidenmüller, and J. Zittartz (Springer-Verlag, Berlin, 1986).
[7]J. Ford, Phys. Today **36** (4), 40 (1983).
[8]S. Smale, Bull. Am. Math. Soc. **73**, 747 (1967).
[9]I. B. Schwartz, Phys. Rev. Lett. **60**, 1359 (1988).
[10]S. D. Stoddard and J. Ford, Phys. Rev. A **8**, 1504 (1973).
[11]S. Nosé, Mol. Phys. **52**, 255 (1984).
[12]S. Nosé, J. Chem. Phys. **81**, 511 (1984).
[13]S. Nosé, Mol. Phys. **57**, 187 (1986).
[14]W. G. Hoover, Phys. Rev. A **31**, 1695 (1985).
[15]D. J. Evans and B. L. Holian, J. Chem. Phys. **83**, 4069 (1985).
[16]W. G. Hoover, A. J. C. Ladd, and B. Moran, Phys. Rev. Lett. **48**, 1818 (1982).
[17]D. J. Evans, J. Chem. Phys. **78**, 3297 (1983).
[18]D. J. Evans, W. G. Hoover, B. H. Failor, B. Moran, and A. J. C. Ladd, Phys. Rev. A **28**, 1016 (1983).
[19]D. J. Evans, in *Molecular-Dynamics Simulation of Statistical-Mechanical Systems,* Proceedings of the International School of Physics "Enrico Fermi," Course XCVII, Varenna, 1985, edited by G. Ciccotti and W. G. Hoover (North-Holland, Amsterdam, 1986).
[20]J. Loschmidt, Sitzungsber. kais. Akad. Wiss. Wien, Math. Naturwiss. Kl. Abt. 2 **73**, 128 (1876).
[21]B. Moran, W. G. Hoover, and S. Bestiale, J. Stat. Phys. **48**, 709 (1987).
[22]G. P. Morriss, Phys. Lett. A **122**, 236 (1987).
[23]G. P. Morriss, Phys. Rev. A **37**, 2118 (1988).
[24]G. P. Morriss (unpublished).
[25]W. G. Hoover, H. A. Posch, and S. Bestiale, J. Chem. Phys. **87**, 6665 (1987).
[26]W. G. Hoover and H. A. Posch, Phys. Lett. A **123**, 227 (1987).
[27]W. T. Ashurst, Ph.D. dissertation, University of California at Davis–Livermore, 1974.
[28]G. Benettin, L. Galgani, A. Giorgilli, and J. M. Strelcyn, C. R. Acad. Sci., Ser. A **286**, 431 (1978).
[29]G. Benettin, L. Galgani, A. Giorgilli, and J. M. Strelcyn, Meccanica **15**, 9 (1980).
[30]I. Shimada and T. Nagashima, Prog. Theor. Phys. **61**, 1605 (1979).
[31]J.-P. Eckmann and D. Ruelle, Rev. Mod. Phys. **57**, 1115 (1985).
[32]A. Wolf, J. B. Swift, H. L. Swinney, and J. A. Vastano, Physica D **16**, 285 (1985).
[33]D. J. Evans, Phys. Rev. A **32**, 2923 (1985).
[34]B. L. Holian, Phys. Rev. A **34**, 4238 (1986).
[35]D. J. Evans and G. P. Morriss, Phys. Rev. Lett. **56**, 2172 (1986).
[36]W. G. Hoover, W. T. Ashurst, and R. J. Olness, J. Chem. Phys. **60**, 4043 (1974).
[37]A. J. C. Ladd, B. Moran, and W. G. Hoover, Phys. Rev. B **34**, 5058 (1986).
[38]R. Livi, A. Politi, and S. Ruffo, J. Phys. A **19**, 2033 (1986).
[39]R. Livi, A. Politi, S. Ruffo, and A. Vulpiani, J. Stat. Phys. **46**, 147 (1987).
[40]D. M. Heyes, G. P. Morriss, and D. J. Evans, J. Chem. Phys. **83**, 4760 (1985).
[41]J. J. Erpenbeck, Phys. Rev. Lett. **52**, 1333 (1984).
[42]H. A. Posch and W. G. Hoover (unpublished).
[43]B. L. Holian and D. J. Evans, J. Chem. Phys. **78**, 5147 (1983).
[44]B. L. Holian, Phys. Rev. Lett. **60**, 1355 (1988).
[45]J. Kaplan and J. Yorke, in *Functional Differential Equations and the Approximation of Fixed Points,* Vol. 730 of *Lecture Notes in Mathematics,* edited by H. O. Peitgen and H. O. Walther (Springer-Verlag, Berlin, 1980).
[46]R. Shaw, Z. Naturforsch. **36a**, 80 (1981).
[47]W. G. Hoover, C. G. Tull, and H. A. Posch, Phys. Lett. A **131**, 211 (1988).
[48]P. Constantin, C. Foias, O. P. Manley, and R. Temann, J Fluid Mech. **150**, 427 (1985).
[49]R. Grappin and J. Leorat, Phys. Rev. Lett. **59**, 1100 (1987).
[50]M. Yamada and K. Ohkitani, Phys. Rev. Lett. **60**, 983 (1988).
[51]L. Keefe, P. Moin, and J. Kim, Bull. Am. Phys. Soc. **32**, 2026 (1987).